

Numerical Simulation of the Interaction between Slender Body Vortices and a Fin

Ashraf A. Omar, Chongam Kim & Oh Hyun Rho

Department of Aerospace Engineering, Seoul National University, Seoul, Korea

ABSTRACT

The interaction between slender body vortices and a single fin located down the axis of the body is investigated numerically for angle of attack of 30 deg. and Reynolds number of 6000. The present research includes a parametric study on the effects of fin axial and azimuthal positions on the development of the vortex system. A numerical method based on the pseudo-compressibility is used for solving the three-dimensional incompressible Navier-Stokes equations using Lower-Upper Symmetric Gauss-Seidel implicit scheme. The numerical results show that the vortices remain very coherent and attached to the body until they reach the fin section where they become less coherent and begin to separate from the body. Also, the result shows that the fin location does not affect the upstream development of the vortices but it does affect the location at which the vortices separate from the body. The effect of azimuthal fin positions was also investigated. As azimuthal angle of the fin increased, the size of the vortex on the port side decreased, but the starboard side vortex grew in size and moved side across the leeward ray to the port side. The computed results are found to agree well with the experimental data.

Keywords: Slender body and fin interaction, asymmetric vortices, steady state, laminar, pseudo-compressibility, LU-SGS algorithms

INTRODUCTION

In numerous applications involving missile, rocket, helicopter, and aircraft aerodynamics, the interaction of vortical flow with control surface plays a very important role in determining the agility and overall performance of craft. Such vortex-control surface interaction, therefore, continues to be the subject of investigation by both experimental and computational modeling 1-3. At lower angle of attacks, these vortices are symmetric, but as the angle of attack increases, the vortices become asymmetric and have different strengths and locations with respect to the missile body. This vortex system may impinge on, or interact with fins or other control surface located further down the missile axis. The interaction is very complex in nature; it can change the pressure field, and, consequently, the loading on these surfaces. This will alter the effectiveness of the surface. In addition, vortex induced loads are difficult to predict and cause changes in yaw, roll, and pitch motions which can be coupled in a nonlinear manner. An investigation to understand the nature and outcome of such interaction is, therefore, of great value.

There has been quite a bit of recent work investigating the interaction between vortical flows and fin surfaces. Acharya *et al.* (1994) conducted experiments to examine the interaction between nose vortex and single fin on various positions along body surface. Their results documented the interaction using flow visualization and mean pressure measurements on the fin surface, where varying degrees of symmetry, preservation or loss of coherence of the incident vortical structures are evident. Nan-Qian Chan's *et al.* (1997) experiment focused on investigating the asymmetric vortices by means of series of configuration; the body alone, the combination of the body and various positions of the wings. Their results include a prediction of vortex induced effect on the side force coefficient. Washburn *et al.* (1997), who examined the effect of tail location

on the vortical flowfield in the wake of a sharp-edged delta wing, observed that no upstream effects on the development or trajectories of the vortices were seen as the position of the tail was changed.

The purpose of the present investigation is to simulate numerically the incident vortex interaction for simplified configuration of a slender body with a single fin, which was considered experimentally (Acharaya *et al.* 1994). The investigation included a parametric study of the effect of the axial location and azimuthal positions of the fin. The flow was considered to be steady and laminar due to experimental conditions (Acharaya *et al.* 1994). An accurate numerical description of the flow required a solution of the in-compressible Navier-Stoke equation. The numerical algorithm is based on the method of artificial compressibility and uses a second order central difference scheme with a third order numerical dissipation (Ok 1993; Yoon and Kwak; Start E. *et al.*). The flow streamlines and the pressure coefficient distribution on both the fin surface is presented. The formation and growth of the vortices, the trajectories of these vortices and the global structure of these vortices at fin section during the interaction are also presented. The computational results are compared with available experimental data.

PROCEDURE

Governing Equations

The three-dimensional incompressible Navier-Stokes equation are solved using the method of pseudo compressibility (Ok 1993; Yoon and Kwak; Start E. *et al.*), which adds a pseudo-time derivative of pressure p to the continuity equation, to make the resultant governing equations hyperbolic, is

$$\frac{\partial p}{\partial \tau} = -\beta \frac{\partial u_j}{\partial x_j} \frac{1}{J} \frac{\partial Q}{\partial \tau} + \frac{\partial}{\partial x_j} (u_i u_j) = -\frac{\partial p}{\partial x_i} + \frac{1}{\text{Re}} \frac{\partial^2 u_i}{\partial x_j \partial x_j} \quad (1)$$

where τ pseudo-time. The above equation can be written in curvilinear coordinates as the following form.

$$\frac{1}{J} \frac{\partial Q}{\partial \tau} = -\frac{\partial}{\partial \xi} (E - E_v) - \frac{\partial}{\partial \eta} (F - F_v) - \frac{\partial}{\partial \zeta} (G - G_v) = -R \quad (2)$$

J is the Jacobian of the transformation; Q is the vector of primitive variable; E , F and G , convective flux vectors; E_v , F_v , G_v , the flux vectors for the viscous term; R is defined as the residual vector of these equations. The variable ξ , η , and ζ describe a curvilinear, body fitted grid.

Numerical Algorithm

The inviscid flux terms are differenced using a second order central differencing scheme with a third order numerical damping. The viscous flux terms are differenced using a second order central difference (Ok 1993). An implicit time integration scheme applied to equation (2) is

$$\frac{Q^{n+1} - Q^n}{\Delta \tau} = -R^{n+1} \quad (3)$$

where the superscript n denotes quantities at the n -th pseudo-time iteration. Pseudo-time step $\Delta\tau$ in equation (3) was calculated by local time step in order to accelerate the convergence. The Lower-Upper Symmetric Gauss-Seidel (LU-SGS) implicit scheme by Yoon and Kwak was used. More detail of the LU-SGS scheme can be found in Yoon & Kwak.

BODY GEOMETRIES AND GRIDS

The body geometry is defined by a 2.6 diameter ogive nose with slender forebody length with the variable location of the fin. The axial locations of the vertical fin are $x/d=4.9$, and 7.1, respectively. The fin has a tapered and clipped delta shape (Fig. 1). This body was tested experimentally by Acharya *et al.* (1994). The results computed on one zone C-O type grid (Fig. 2), which are generated by rotating a two-dimensional C-type grid encompassing the contours of the ogive slender around its longitude axis. Outer boundary of computational domain is located at $R/d=28$. This radial extent of the

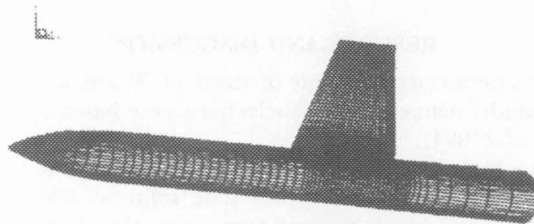


Fig. 1. Surface grid for a tangent-ogive body with a fin at $(x/d)=7.1$

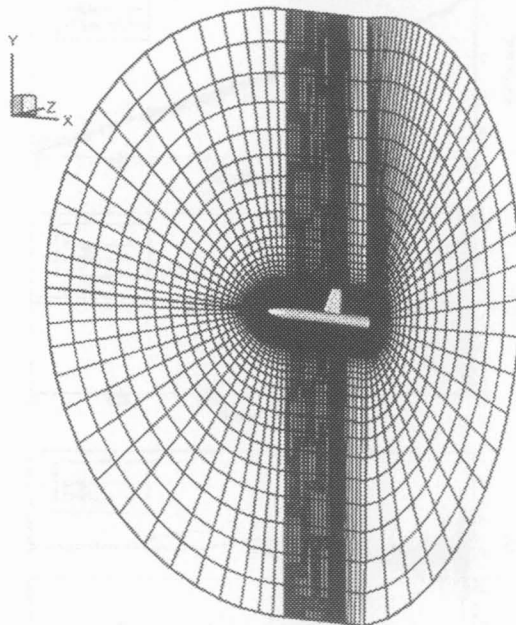


Fig. 2. Full view of the computational grid

computational domain ensures that a solution is less susceptible to the far field boundary condition. Two different physical grid points are used for computation; grid A, as shown in Fig. 2, is consisted of 75x81x71 points for body with axial fin position equal to 7.1, and grid B of 65x81x71 points with axial fin position equal to 4.9. Grid was clustered to the body and fin surface to resolve boundary layer and circumferential grid spacing is concentrated on the leeward surface where vortices are expected to exist. For a fin placed at azimuthal angle greater than zero (non-vertical fin), the zero azimuthal angle (vertical fin) grid was rotated to new azimuthal angle.

Initial and Boundary Condition

Freestream values are specified at far boundaries, while out flow boundary is extrapolated using zeroth order extrapolation. Pressure is kept its free stream value. On a solid surface, usual no slip condition is applied. The pressure at the solid surface is obtained by setting the pressure gradient normal to the wall to be zero. Unknown value of Q on the boundaries are updated explicitly.

RESULTS AND DISCUSSION

The computation was performed for angle of attack of 30 deg. and Reynolds number of 6000 based on the model diameter. These selections were based upon the experimental work by Acharya *et al.* (1994).

The convergence history summarized in Fig. 3 discloses that the vortical flowfield results for both cases indeed reach a steady state solution. Shown in Fig. 3 are the convergence histories of residual, normal force, and side force. It is seen that the

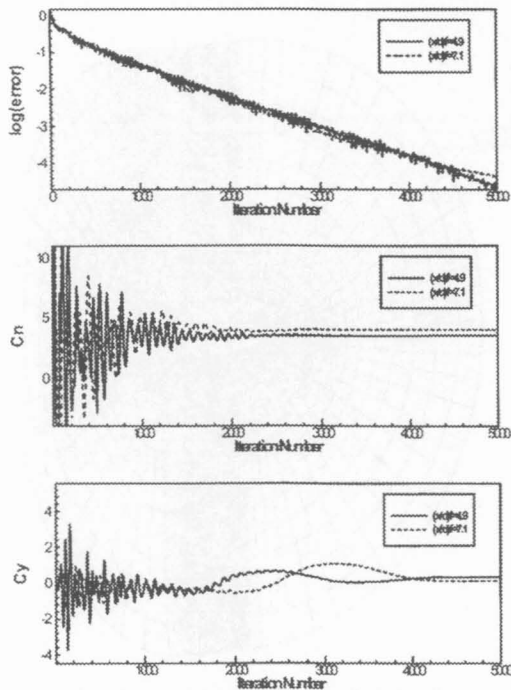


Fig. 3. Convergence histories: $\Phi_f = 0^\circ$

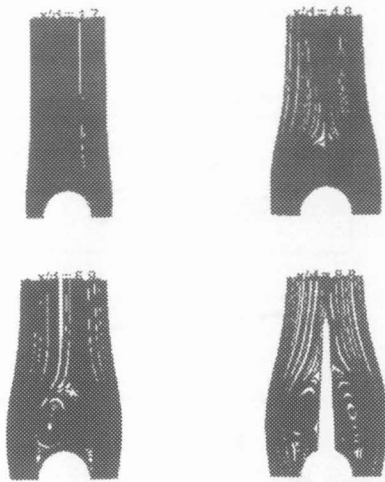


Fig. 4. Cross sectional flow streamlines:
(x/d) $f=7.1$

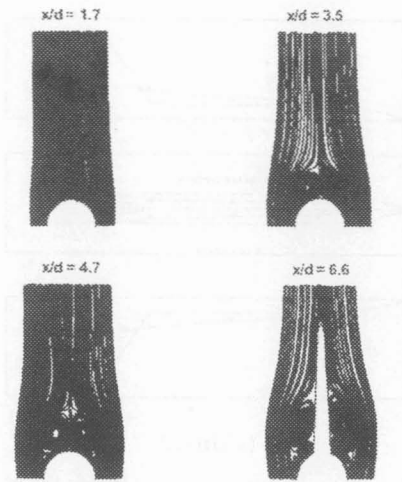


Fig. 5. Cross sectional flow streamlines:
(x/d) $f=4.9$

residual is dropped below four orders of magnitude within about 4500 iteration. Fig. 4 shows the development of the flow along axial location of the body when the fin is located at $x/d=7.1$. At axial location close to the nose ($x/d=1.7$), the pair of the vortices has formed symmetrical, coherent and attached to the body. They remain largely coherent, and attached to the body through $x/d=4.9$. At $x/d=6.9$, near the leading edge of the fin, the degree of asymmetry increases where the left side primary vortex starts to leave away from the body due to presence of the fin, and the right side vortex still increasing in size and attached to the body. At $x/d=8.8$, in the middle of the fin, the primary vortices are far away from the body. At this position, secondary vortices appear so clearly and it is big in size due the interaction with corner flow. At $x/d=9.4$, trailing edge of the fin (not shown here), the vortices are keeping a same shape with little increase in the size. The comparison between the computational streamlines and experimental visualization photograph by Acharaya *et al.* (1994) shows good agreement. The flowfield develops similarly with a fin placed at axial location equal to 4.9 diameter as shown in Fig. 5. As the fin is positioned closer to the nose, the vortices are smaller in size when they come in contact with the fin. Therefore, while the axial location of the fin does not affect the upstream development of the vortices, it does affect the location at which vortices separate from the body. No vortex breakdown was observed in either the present study or the experiment (Acharaya *et al.* 1994). A comparison of the location of primary vortices center between the experiment (Acharaya *et al.* 1994) and the computation is shown in Figs. 6.a and 6.b. Good agreement is obtained. These figures show that the trajectories of the port and the starboard side vortices are almost the same in each, confirming the symmetry of the trajectories of the vortices. These figures show clearly that the axial location of the fin dose not affect the development of the flowfield.

The surface pressure coefficient contours for the axial fin position of $x/d=7.1$ and 4.9 are shown in Figs. 7.a and 7.b, respectively. In these figures, dashed line indicates a negative C_p , while solid line a positive C_p . Fig. 7.a shows C_p contour in both sides of the fin located at $x/d=7.1$. A large low-pressure region, which is seen between the fin root and half span, is the consequence of the primary and secondary vortices. As seen

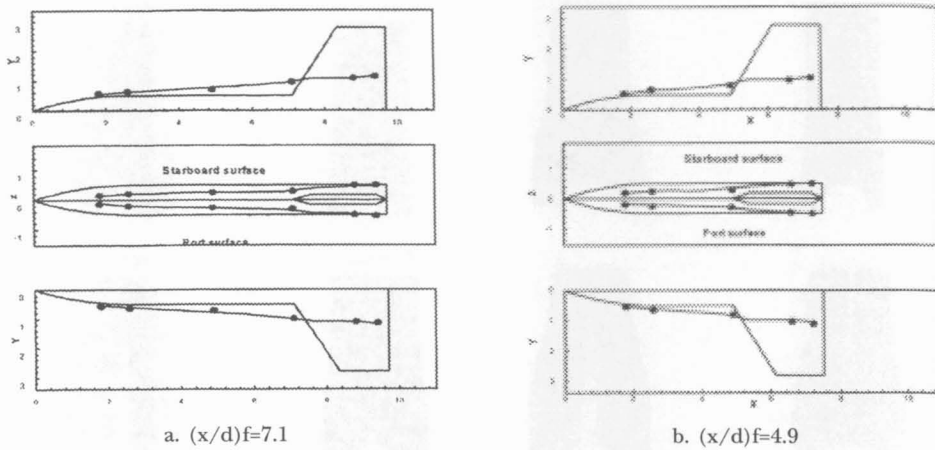


Fig. 6. Vortex center trajectories: $\Phi_f=0$

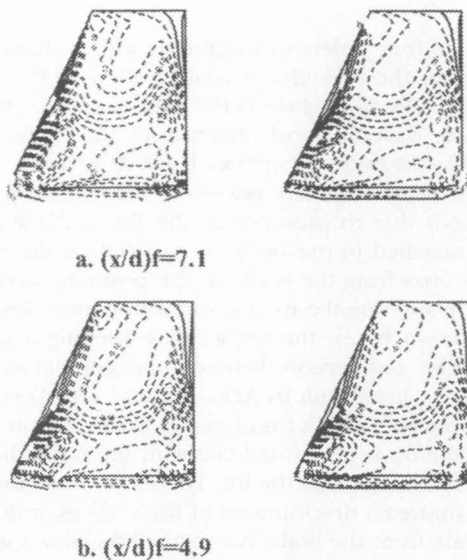


Fig. 7. Pressure coefficient contours on fin: $\Phi_f=0^\circ$

in Fig. 4, at $x/d=8.8$, the center of the two primary vortices pass on either side of the fin slightly inboard of the half span with secondary vortices on the fin-body corner, they creating a region of low pressure between the fin root and half-span. At half-span, contours show a rapid rise in pressure in spanwise direction due to flow toward the fin surface. The fin surface pressure coefficient contour shown in Fig. 7.b for fin at $x/d=4.9$ is similar but the low pressure region is small in spanwise extent and close to fin root due to the small size and location of the primary vortex.

A combination of high angle of attack and asymmetrical azimuthal angle of the fin produces very complex vortical flow on fin section. Therefore, one of the concerns of

the present study is to investigate the effect of the azimuthal position of the fin on the flow development and pressure distribution contour on both sides of the fin. The solution obtained for the same bodies and flow conditions is described for vertical fin. The fin was rotated to several azimuthal positions; $\phi_f=6^\circ$, 11° and 16° , where $\phi_f=0^\circ$ refers to the vertical fin, ϕ_f being positive clock-wise. For each azimuthal position of the fin, the numerical results reached steady flowfields.

In the first case, the fin located at $x/d=7.1$, Figs. 8.a, 8.b and 8.c show the flow development along the missile body when the fin azimuthal positions are 6° , 11° and 16° , respectively. There are no apparent effects of the azimuthal fin position on the structures and the trajectories of the vortices upstream of the fin section. The effect of the fin azimuthal position is only altered once they reach the fin section. The experimental flow visualization by Acharya *et al.* 1994 also showed a similar trend. At both axial fin locations ($(x/d) f=4.9$ and 7.1), the azimuthal position of the fin changes the relative distance between each vortex and the fin surface. The trajectories of the vortices on the fin are also affected by the azimuthal position of the fin. At axial location ahead of fin's leading edge, the vortices appear very similar to those shown in Figs. 4 and 5 (vertical

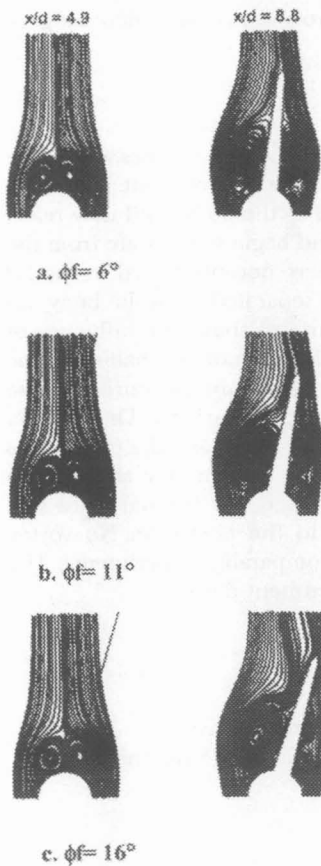


Fig. 8. Effect of the fin azimuthal positions on flow development: $(x/d) f = 7.1$

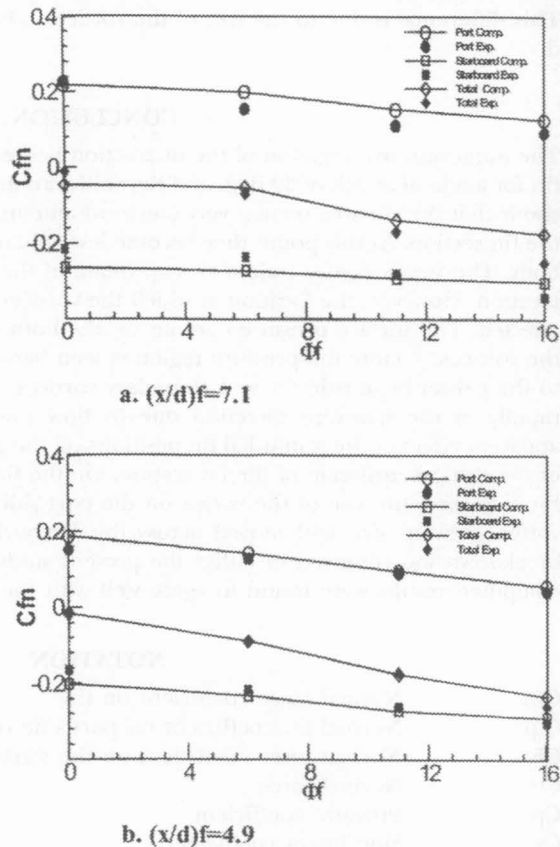


Fig. 9. Variation of normal force coefficient on fin with ϕ_f

fin). On the fin section, as azimuthal angle of the fin increases, the size of the vortices on the port side decreases and the starboard side primary vortices grow in size and move across the leeward ray to the port side of the body.

The effect of the vortex system can be clearly shown by studying the normal force on the fin. Fig. 9 shows the variation of the normal force on the fin with azimuthal position of the fin at each fin location. Shown are the components on the port side and starboard side surface (C_{fp} and C_{fs} , respectively). Overall, computed results agree fairly well with experimental data (Acharya *et al.* 1994). The outward normal to the port side of the fin is assumed to be positive direction according to experimental condition (Acharya *et al.* 1994). For each fin position ($(x/d) f=4.9$ and $(x/d) f=7.1$), the force is nearly anti-symmetric about $\phi f=0$, where total force is close to zero. As azimuthal position of the fin (ϕf) increases, the magnitude of the C_{fp} on the port side decreases due to a decrease in the vortex effect on the fin while the magnitude of C_{fs} on the starboard side increases. Also, the total normal force coefficient on the fin shows that the degree of asymmetry increases as azimuthal position of the fin increases. The variation of C_f is similar at both axial fin positions but slightly different in the magnitude of the normal force. As fin is placed at $x/d=7.1$, the normal force is larger than the case of $(x/d)f=4.9$. This difference is due to the size of the vortices, which grow in size with increasing x/d .

CONCLUSION

The numerical investigation of the interaction between slender body vortices and single fin for angle of attack of 30 deg. and Reynolds number of 6000 is carried out. The study shows that the vortices remain very coherent and attached to the body until they reach the fin section. At this point, they become less coherent and begin to separate from the body. The vortex center trajectories upstream of the fin were not influenced by the fin location. However, the location at which the vortices were separated from the body was affected. The surface pressure contour on the both fin surfaces shows the influence of the vortices. A large low-pressure region is seen between the fin root and half-span due to the existence of primary and secondary vortices. At half-span, the pressure increase rapidly in the spanwise direction due to flow toward the fin surface. There is no apparent effect of the azimuthal fin positions on the global structure and the trajectories of the vortices upstream of the fin section. On the fin section, as azimuthal angle of the fin increased, the size of the vortex on the port side decreased, but the starboard side vortex grew in size and moved across the leeward ray to the port side. No vortex breakdown was observed in either the present study or comparable experiments. The computed results were found to agree well with the experiment data.

NOTATION

C_{fn}	Normal force coefficient on fin
C_{fp}	Normal fin coefficient on port side of the fin (positive)
C_{fs}	Normal force coefficient on the starboard side of the fin (negative)
C_n	Normal force
C_p	Pressure coefficient
C_y	Side forces coefficient
E, F, G	Inviscid flux vectors
E_v, F_v, G_v	Viscous flux vectors
J	Jacobian
n	Time level

P	Pressure
Q	Vector of primitive variables
R	Residual
u_i	Velocity
x_i	Carestrain coordinate
x/d	Dimensionless distance from the nose
$(x/d)f$	Dimensionless distance from the nose to leading edge of the fin
ξ, η, ζ	Generalized curvilinear coordinate
$\Delta\tau$	Pseudo-time step
ϕf	Azimuthal angle of the fin

REFERENCES

- ACHARAYA, M., J. KIEDAISCH and M. MOHAMMAD HASSAN. 1994. "Asymmetry vortical flows over slender bodies with appendage," ITT Fluid Dynamics Research Center, TR, Chicago, IL, June 1994.
- HONAM OK. Development of an Incompressible Navier-Stokes solver and its application to the calculation of separated flows. Ph.D Dissertation, Department of Aeronautical and Astronautics, University of Washington, 1993.
- MENDENHALL, M. R., and PERKINS, S. C., Jr. "Vortex Induced Characteristics of Missiles in Unsteady Maneuvers," AIAA Paper 89-0344, Jan 1989.
- NAN-QIAN CHAN, ZHEN-YU WANG and ZHENG HUANG. Asymmetric Vortices and Alleviation on the Slender Bodies with and without Wings. AIAA Paper 97-0748, 1997.
- ROGERS START E. , DOCHAN KWAK and CETIN KIRIS. 1991. Steady and unsteady solutions of the incompressible Navier-Stokes equations. *AIAA Journal* **29(4)**: 603-610.
- YOON SEOKKWAN and DOCHEN KWAK "Three dimension incompressible Navier-Stokes Solver using Lower-Upper-Gauss-Seidel Algorithm." *AIAA Journal* **29(6)**: 874-875.
- WASHBURN, A. E., L. N. JENKINS and M. A. FERMAN. Experimental Investigation of Vortex-Fin Interaction. AIAA Paper 93-0050, Jan. 1993.